Journal of Solid State Electrochemistry (2020) 24:655–665
https://doi.org/10.1007/s10008-020-04507-3

ORIGINAL PAPER

Effect of $Mg(CF_3SO_3)_2$ concentration on structural and electrochemical properties of ionic liquid incorporated polymer electrolyte membranes

C. Maheshwaran[1] · D.K. Kanchan[1] · Khushbu Gohel[1] · Kuldeep Mishra[2] · Deepak Kumar[3]

Received: 4 October 2019 / Revised: 11 December 2019 / Accepted: 17 January 2020 / Published online: 21 January 2020

Abstract

In the present study, a magnesium ion conducting polymer electrolyte membrane system based on polyethylene oxide (PEO) containing magnesium triflate $Mg(CF_3SO_3)_2$ salt and 1-ethyl-3-methylimidazolium tetrafluoroborate (EMIM-BF_4) ionic liquid is prepared using standard solution casting technique. X-ray diffraction and differential scanning calorimetry studies reveal change in crystalline character with variation in $Mg(CF_3SO_3)_2$ concentration within PEMs. Fourier transform infrared spectroscopy technique reflects ion-polymer interactions within the prepared polymer electrolyte system. Dielectric and modulus properties of prepared electrolyte membranes show significant changes in dielectric constant and relaxation behavior respectively on varying $Mg(CF_3SO_3)_2$ concentration. The optimized polymer electrolyte membrane with 6 wt% of magnesium triflate salt shows maximum ionic conductivity of $\sim 9.4 \times 10^{-5}$ S cm^{-1} at room temperature. The ionic conductivity variation with temperature shows Arrhenius behavior for PEMs. The Mg^{2+} conduction within the PEMs is established using CV study and electrochemical stability window of ~ 4.0 V is determined using linear sweep voltammetry. The PEMs are dominantly ionic conducting with Mg^{2+} transport number ~ 0.22 for the optimized PEM.

Keywords Polymer electrolyte membranes · Mg ion conductor · Ionic liquid · Ionic conductivity

Introduction

Since the commercialization of first lithium-ion battery in 1991, these batteries, with two Li^+ insertion electrodes and a Li-ion conducting electrolyte, have been established as an ultimate sophisticated energy storage device [1–3]. However, the high cost, less abundance, environmental impacts, and some safety limitations have forced the researchers to look for alternate electrochemical cells based on Na, Mg, Zn, K, Al, etc. [4–9]. Magnesium, with $E°$ of − 1.55 V vs SHE and theoretical capacity of 2205 mA h g^{-1}, appears a good substitute of Li-ion batteries [10]. Further, the cost effectiveness, low toxicity, ease of handling, and lesser reactivity of magnesium make it attractive for fabricating electrochemical devices such as batteries, fuel cells, supercapacitors, solar cells, and electrochemical displays. For realizing commercial Mg-ion batteries, a good ion conducting electrolyte with significant electrochemical and thermal stability is a prerequisite [11].

Polymer electrolyte membranes (PEMs) have recently attracted much attention for applications in energy storage and conversion devices [12, 13]. For fabrication of PEM, various polymers such as poly ethylene oxide (PEO), poly(vinylidene fluoride-co-hexafluoropropylene) (PVDF-HFP), poly(methyl methacrylate) (PMMA), polyvinyl alcohol (PVA), polyvinyl chloride (PVC), polyvinylpyrrolidone (PVP), polyacrylonitrile (PAN), rubber (MG49, ENR50, etc.), polyester, and polycarbonate are utilized. PEO-based PEMs have been extensively reported for various electrochemical devices including the magnesium-ion batteries [14–16]. PEO-based PEMs own low ionic conductivity due to its semi-crystalline nature which seized the segmental motion of polymer chain and restrict the ion mobility. The researchers have attempted to suppress the crystallinity of the

✉ Deepak Kumar
fwtdrdeepak@gmail.com; deepak.kumar06@gov.in

[1] Department of Physics, M.S. University of Baroda, Vadodara, Gujarat 390002, India

[2] Department of Physics, Jaypee University, Anoopshahr, Uttar Pradesh 203390, India

[3] Electronics and Mechanical Engineering School (Affiliated to Gujarat Technological University), Under Corps of EME, Ministry of Defence, Vadodara, Gujarat 390008, India

PEO chain to improve mobility of ions through faster ion hoping, thereby leading to better ionic conduction. The ion hopping is believed to be predominant in amorphous PEO-based PEMs [17].

An alternative method of achieving high conductivity while retaining the useful properties of PEMs is to use ionic liquids (ILs) either as the main conducting species immobilized in a polymer membrane or as a plasticizing agent in the PEMs [18, 19]. The 1-ethyl-3-methylimidazolium tetrafluoroborate (EMIM-BF_4) ionic liquid is a green solvent, which acts as plasticizer and supplier of new charge carriers (bulky and asymmetric organic $EMIM^+$ cations and inorganic BF_4^- anions) for ionic conduction in polymer electrolyte system. This ionic liquid possesses various specific properties such as wide liquid-phase range, non-volatility, non-flammability, eco-friendliness, ability to dissolve in a variety of compounds, negligible vapor pressure at room temperature, wide electrochemical stability window, high ionic conductivity, and excellent thermal/chemical stability [19, 20].

The ion conduction mechanism in polymer electrolytes has been explained by various models [21]. The role of ILs in electrolytic properties of PEO-based Li-ion conducting PEMs has been investigated by Chaurasia et al. [22, 23]. They demonstrated that the IL confined in PEO not only plasticizes the polymer but also coordinates with the electronegative group of PEO and influences free ion concentration within PEM. However, the reports on Mg^{2+}-based PEMs lack in numbers when compared with the existing Li-ion- and Na-ion-based PEMs [6, 24–30]. It is important to note that researchers are trying hard to develop a commercial Mg-ion conducting electrolyte by using ionic liquids as non-flammable molten salts and active/passive nanofillers for better solvent retention within the polymer-based electrolyte systems [31, 32]. The study of ion-dynamics behavior in such PEMs is of fundamental interest to fabricate modern electrolyte systems by tailoring conduction mechanism. However, a systematic study for understanding the role of IL in modifying the structural and electrochemical properties of Mg^{2+} conducting PEM is still lacking. Here, we present a detailed analysis of Mg^{2+} conducting PEMs using PEO and EMIM-BF_4 as ionic liquid with varying concentrations of $Mg(CF_3SO_3)_2$ salt. EMIM-BF_4 is known as moisture-stable form of IL. $EMIM^+$ cation if combined with $CF_3SO_3^-$ anion of $Mg(CF_3SO_3)_2$ also forms EMIM-CF_3SO_3 as moisture-stable forms of IL [33, 34]. Considering the low viscosity (2 cP), high conductivity (15.92 mS cm^{-1}), and high dielectric constant (14.8), we have taken (EMIM-BF_4) IL compared to other imidazole-based ILs. Enhancement of ionic conductivity occurs due to ionic dissociation through Lewis acid–base interaction between IL and polymer/ionic species. In view of this, it would be interesting study to investigate the structural and electrochemical properties of PEMs containing $EMIMBF_4$ as ionic liquid, PEO as polymer host, and $Mg(CF_3SO_3)_2$ as salt.

In this study, we have shown how the salt changes/controls ionic conduction and relaxation parameters in polymer electrolyte for electrochemical performances with these electrolytes.

Experimental section

Materials

The materials used for the preparation of PEMs were PEO of average molecular weight ~ 300,000 from Alfa Aesar, magnesium triflate, $Mg(CF_3SO_3)_2$, salt of 97% purity from Aldrich, and EMIM-BF_4 extrapure for catalysis and nanotechnology grade from SRL. Acetone of purity 99% was obtained from Aldrich and was used as received for dissolving polymer host.

Preparation of PEMs

PEMs were prepared by standard solution casting technique. In this technique, initially stoichiometric amounts of polymer PEO and ionic liquid EMIM-BF_4 (9:1 wt/wt) were dissolved in acetone through continuous stirring for 5–6 h at 40 °C. The homogeneous solution, thus obtained, was poured in Teflon petri dish and left for solvent evaporation at ambient temperature. After complete evaporation of the solvent, free standing membrane containing no magnesium salt was obtained. In order to obtain Mg^{2+} conducting PEM, the various concentrations of $Mg(CF_3SO_3)_2$ salt were added to the PEO + EMIM-BF_4 solution according to compositional formula; (PEO + EMIM-BF_4) + x wt% $Mg(CF_3SO_3)_2$ for $x = 1$ to 7 wt%. After complete evaporation of the solvent, Mg^{2+} conducting free standing PEMs were obtained.

Characterization of PEMs

X-ray diffraction measurements were carried out with XPERT-PRO System using CuKα radiation in the Bragg angle (2θ) ranging from 10° to 70° at scanning rate of 2° min^{-1}. Atomic force microscopy was performed by employing AFM, pico SPM-picoscan 2100, Molecular Imaging, USA. The imaging was performed in tapping mode with a diamond-like carbon coated ultra-sharp silicon tip. Fourier transform infrared spectra of the prepared samples were recorded in the wavenumber range of 650–4000 cm^{-1} using single beam FTIR 4100 JASCO model. The spectra were recorded by averaging 32 scans per sample with an optical resolution of 4 cm^{-1}. The measurements were taken by directly mounting the electrolyte membrane in the sample holder in transmission mode. Thermal properties of these PEMs were studied by differential scanning calorimetry (DSC). For the DSC measurement, samples were hermetically sealed in aluminum pan and DSC thermograms were obtained in the temperature range from RT to 70 °C using

SII EXSTAR-6000 systems at the heating rate of 10 °C min^{-1} under N_2 atmosphere. The electrical characterization of PEMs was performed by impedance spectroscopic technique. Precision Solartron 1260 Impedance analyzer was used in the frequency range from of 1 Hz to 32 MHz with a signal level of 50 mV in temperatures range from 303 and 333 K. The impedance measurements are carried out by sandwiching the PEMs between two stainless steel electrodes under spring pressure. The cyclic voltammetry (CV) and linear sweep voltammetry (LSV) were performed by using electrochemical analyzer (Zive SP1) of WonATech Co., Ltd., Korea at scan rate of 5 mV s^{-1}. The dc polarization measurements were also performed by using electrochemical analyzer (Zive SP1) of WonATech Co., Ltd., Korea.

Results and discussion

X-ray diffraction studies

X-ray diffraction (XRD) patterns have been recorded and shown in Fig. 1 for various $Mg(CF_3SO_3)_2$ salt concentration within the PEMs. The polymer electrolyte consisting of PEO and ionic liquid EMIM-BF_4 shows peaks at 19.6°, 23.4°, and 27.0°, respectively, due to the semi-crystalline nature of PEO polymer. PEMs consisting of PEO + EMIM-BF_4 with varying amount of $Mg(CF_3SO_3)_2$ salt maintain the prominent peaks orientation at 19.6° and 23.4°, respectively [35]. It is important to note that the peak intensity corresponding to 19.6° and 23.4° reduces on increasing the concentration of $Mg(CF_3SO_3)_2$ salt from 0 to 6 wt%. This decrease in peak intensity can be inferred as possible decrease in crystalline character of the PEMs on enhancing the $Mg(CF_3SO_3)_2$ salt concentration. When the $Mg(CF_3SO_3)_2$ salt concentration reaches to 7 wt%, an increase in peak intensity is observed which depicts the rise in crystalline character of the PEMs. Thus, significant structural changes are observed when $Mg(CF_3SO_3)_2$ salt concentration changes within the polymer electrolyte membranes [36].

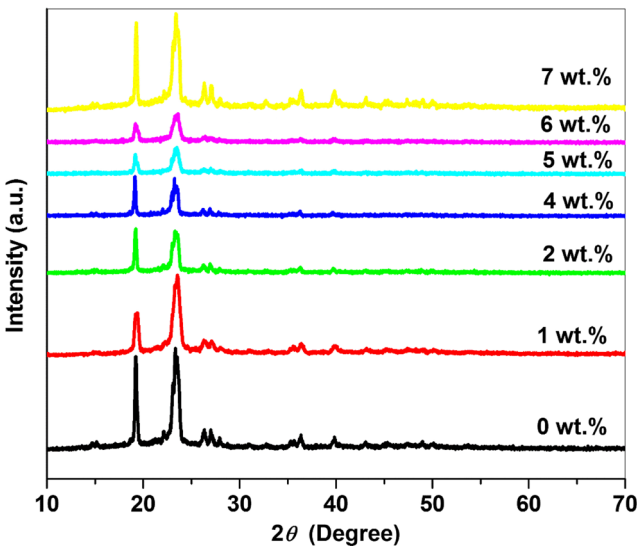

Fig. 1 X-ray diffraction patterns of PEO + EMIMBF_4 with varying amount of $Mg(CF_3SO_3)_2$ salt from 0 to 7 wt%

AFM studies

Figure 2 displays the AFM micrographs of the PEMs consisting of PEO, EMIM-BF_4, and $Mg(CF_3SO_3)_2$ salt. On varying $Mg(CF_3SO_3)_2$ salt concentration within the PEMs, significant morphological changes are observed with respect of roughness events as seen in Fig. 2a–d . On addition of $Mg(CF_3SO_3)_2$ salt concentration from 1 to 6 wt% in PEO + EMIM-BF_4 matrix, the maximum roughness height in AFM graphs changes from 794 to 148 nm while an average roughness height decreases from 340 to 90 nm, respectively. This

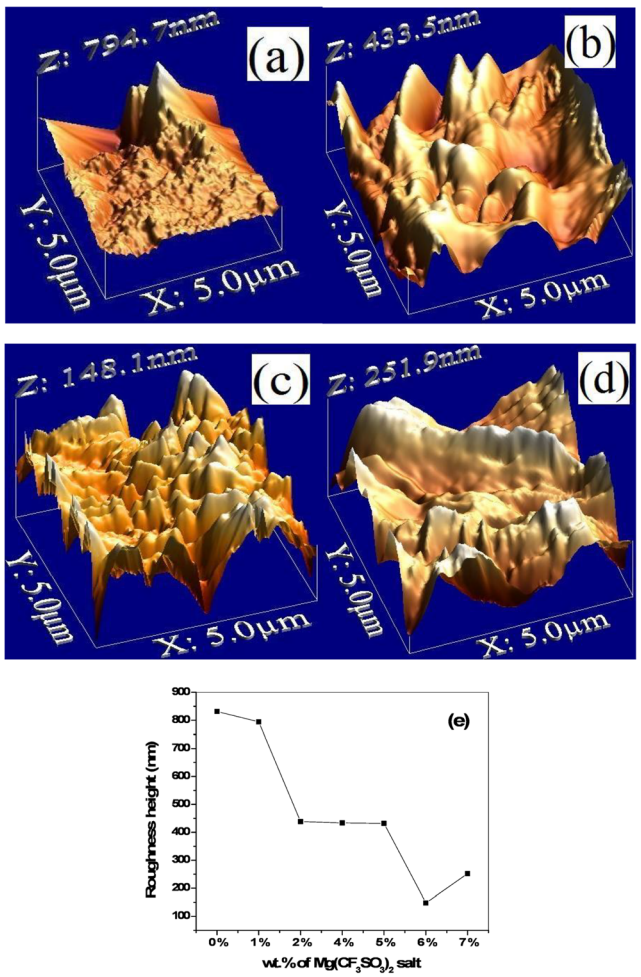

Fig. 2 AFM analysis for PEMs with composition (PEO + EMIM-BF_4) + x wt% $Mg(CF_3SO_3)_2$: **a** $x = 1$, **b** $x = 5$, **c** $x = 6$, **d** $x = 7$, and **e** roughness height verses $Mg(CF_3SO_3)_2$ salt concentration

reduction in roughness peaks is possibly due to initial supportive aggregation of ions from $Mg(CF_3SO_3)_2$ and EMIM-BF_4 occupying the conduction pathways inside the PEO + EMIM-BF_4 matrix [37]. However, at 7 wt% of $Mg(CF_3SO_3)_2$ salt concentration, the maximum roughness height dramatically rises to 251 nm and average roughness height to 125 nm as shown in Fig. 2e . The sudden rise in height of roughness events may be due to blocking effects of salt aggregation as explained by Parthiban et al. [38].

FTIR studies

In order to investigate any change in molecular bond lengths and/or interaction among PEO, EMIM-BF_4, and $Mg(CF_3SO_3)_2$ salt in PEMs, FTIR spectra of pure PEO, (EMIM-BF_4) IL, $Mg(CF_3SO_3)_2$ salt, and (PEO + EMIM-BF_4) + $Mg(CF_3SO_3)_2$ PEMs have been obtained (Fig. 3a). The constituent materials are showing their characteristic bands. The polymer PEO has ethylene group (-CH_2-CH_2-), which shows different twisting, wagging, and rocking type vibrations. The C-O-C group attached to the main chain of PEO possesses symmetric and asymmetric vibration modes with a tendency of forming hydrogen bond with the cation of the ionic liquid EMIM-BF_4 and salt $Mg(CF_3SO_3)_2$ [22]. Thus, the immobilization of EMIM-BF_4 and $Mg(CF_3SO_3)_2$ in PEO may lead significant changes in these IR active modes of PEO. In order to see the effect of addition of IL in PEO with subsequently variation of salt $Mg(CF_3SO_3)_2$ in PEO + EMIM-BF_4, the FTIR spectra of PEO, EMIM-BF_4, $Mg(CF_3SO_3)_2$ salt, PEO with EMIM-BF_4 membrane, and (PEO + EMIM-BF_4) with 6 wt% $Mg(CF_3SO_3)_2$ PEM have been extended because main features are observed in the wavenumber region 700–1700 cm^{-1} (Fig. 3b). The changes in the following features are observed:

(i) The bands at 744 cm^{-1} of C-H bending in pure PEO disappear when IL is added to PEO and (PEO + EMIM-BF_4) + $Mg(CF_3SO_3)_2$ PEMs.

(ii) The band at 840 cm^{-1} of C-O stretching in pure PEO has been shifted to 844 cm^{-1} when $Mg(CF_3SO_3)_2$ salt is increased in the (PEO + EMIM-BF_4) + $Mg(CF_3SO_3)_2$ PEM.

(iii) The bands observed in the region 1000–1200 cm^{-1} corresponding to the C-O-C stretching vibration of PEO are very much sensitive to the cations of both the ionic liquid $EMIM^+$ and Mg^{2+} [36, 39]. The PEO shows characteristic bands at 1009, 1057, 1100, and 1146 cm^{-1} in this region. The band at 1009 cm^{-1} also disappears in (PEO + EMIM-BF_4) + $Mg(CF_3SO_3)_2$ PEM due to addition of IL which is showing a broad flat dip in this region. However, the bands at 1057 and 1146 cm^{-1} of pure PEO have been shifted to 1061 and 1149 cm^{-1}, respectively, when the IL is immobilized in PEO. The band at 1100 cm^{-1} in pure PEO shifts to 1109 cm^{-1} even in (PEO + EMIM-BF_4) membrane as well as in (PEO + EMIM-BF_4) + $Mg(CF_3SO_3)_2$ PEM. These observations suggest the possible interaction of the $EMIM^+$ of IL and Mg^{2+} of salt with ether oxygen of PEO.

(iv) Additionally, the band at 1276 cm^{-1} of pure PEO is observed to shift at 1282 and 1280 cm^{-1} while the band at 1635 cm^{-1} of C=C and C=N stretching of pure IL appears to shift to higher wave number side, i.e., 1656 cm^{-1} in all PEM membranes. It means the bond lengths of C=C and C=N stretching of pure IL slightly decrease due to the interaction with PEO and Mg salt in the PEMs.

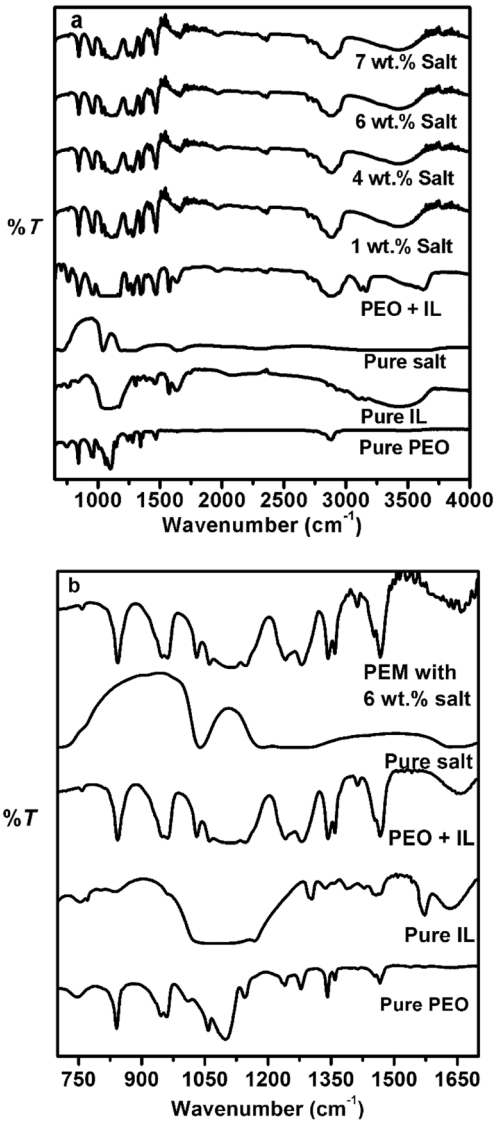

Fig. 3 **a** FTIR spectra of pure PEO, pure EMIM-BF_4 IL, pure $Mg(CF_3SO_3)_2$ salt, PEO + EMIM-BF_4 membrane, and PEO + EMIM-BF_4 containing different $Mg(CF_3SO_3)_2$ concentrations; **b** extended FTIR spectra of pure PEO, pure EMIM-BF_4 IL, PEO + EMIM-BF_4 membrane, pure $Mg(CF_3SO_3)_2$ salt, and PEO + EMIM-BF_4 containing 6 wt% $Mg(CF_3SO_3)_2$ salt in the wavenumber range 700–1700 cm^{-1}

(v) The bands centered at 1298 and 1571 cm^{-1} of pure IL disappear in the IR spectra of (PEO + EMIM-BF_4) + $Mg(CF_3SO_3)_2$ PEMs.

(vi) No separate bands of pure $Mg(CF_3SO_3)_2$ salt have been observed in PEMs, which is indicative of the complete complexation of the salt.

In addition to these observations, the broad band centered at ~ 3440 cm^{-1} in pure EMIM-BF_4 IL is due to the symmetric stretching of the aromatic ring of IL observed in all the PEMs at all salt concentrations [40]. However, this band appears narrower in (PEO + EMIM-BF_4) + $Mg(CF_3SO_3)_2$ PEMs (Fig. 3a). It is well known that the –OH stretching also gives its signature in IR near 3200 cm^{-1} wavenumber which may be due to the hygroscopic nature of $Mg(CF_3SO_3)_2$ salt in the PEMs. But as this peak is centered away from 3400 cm^{-1} and no change in shift is observed with the addition of $Mg(CF_3SO_3)_2$ salt in any of these PEMs, hence presence of –OH stretching vibrations is neglected. These observations suggest the good complexation among PEO, EMIM-BF_4, and $Mg(CF_3SO_3)_2$ in PEMs.

DSC analysis

DSC has been utilized to probe the amorphous or crystalline nature of PEMs membranes. Figure 4 shows the DSC thermograms for the electrolyte system PEO + EMIM-BF_4 with varying amount of $Mg(CF_3SO_3)_2$ salt. The reduction in melting temperature (T_m) is observed with the increasing concentration of $Mg(CF_3SO_3)_2$ till 6 wt%. In addition, the broadening of the peaks with salt concentration enhancement is evident from the thermogram which is indicative of increase in amorphous nature within PEMs.

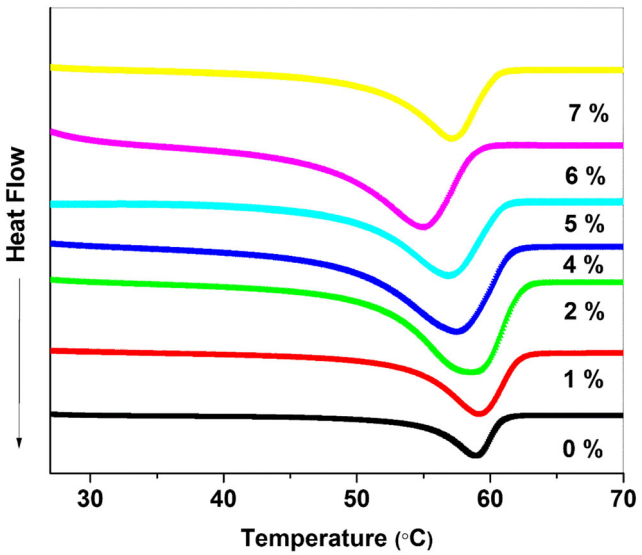

Fig. 4 DSC curves of PEO + EMIM-BF_4 and PEO + EMIM-BF_4 containing different concentrations of $Mg(CF_3SO_3)_2$

The decrease in T_m of polymer with increasing amounts of the $Mg(CF_3SO_3)_2$ leads to the flexible polymer backbone due to the weaker intermolecular interaction between polymer chains. This flexible polymer backbone facilitates higher segmental motion of the polymer backbone and hence high ionic conductivity [25]. Further, the reduction of melting temperature and broadening of melting endothermic peaks with the addition of $Mg(CF_3SO_3)_2$ salt are consistent with increase in the amorphous phase of PEMs which are in consonance with results of XRD pattern. The degree of crystallinity (X_c) is calculated for 100% crystalline PEO phase by the Eq. 1 [41] and results are presented in Table 1.

$$X_c = \left(\frac{\Delta H_m}{\Delta H_m^o}\right) \times 100\% \quad (1)$$

Here ΔH_m^o and ΔH_m are the melting enthalpy of 100% crystalline PEO and prepared PEMs. The endothermic peaks corresponding to melting temperature (T_m) are also indicated in Table 1. It can be noticed that T_m peaks shift towards lower values till 6 wt% concentration of the $Mg(CF_3SO_3)_2$ salt. This change has been attributed to the possible plasticization effect of EMIM-BF_4 ionic liquid [42].

Electrochemical impedance spectroscopy

Nyquist plots and ionic conductivity

The Nyquist plot (Z' vs Z'') for the freshly prepared PEMs with different $Mg(CF_3SO_3)_2$ concentration at temperature 303 K is shown in Fig. 5a . The difference between real part of impedance at high frequency and low frequency end of semicircular portion indicates the bulk resistance (R_b) of the PEMs. From Fig. 5a , we observe that the R_b decreases as the $Mg(CF_3SO_3)_2$ salt concentration increases from 0 to 6 wt%. However, R_b slightly increases for 7 wt% salt concentration. The R_b is inversely proportional to the ionic conductivity and is given by the formula

Table 1 Melting temperature (T_m) and degree of crystallinity (X_c) of PEO + EMIM-BF_4 with increasing $Mg(CF_3SO_3)_2$ concentration

(PEO + EMIM-BF_4) + x wt% $Mg(CF_3SO_3)_2$	T_m (°C)	%X_c
$x = 0$	59.2	52.5
$x = 1$	58.9	46.2
$x = 2$	58.5	35.2
$x = 4$	57.5	33.3
$x = 5$	56.5	28.4
$x = 6$	54.9	16.3
$x = 7$	57.0	35.2

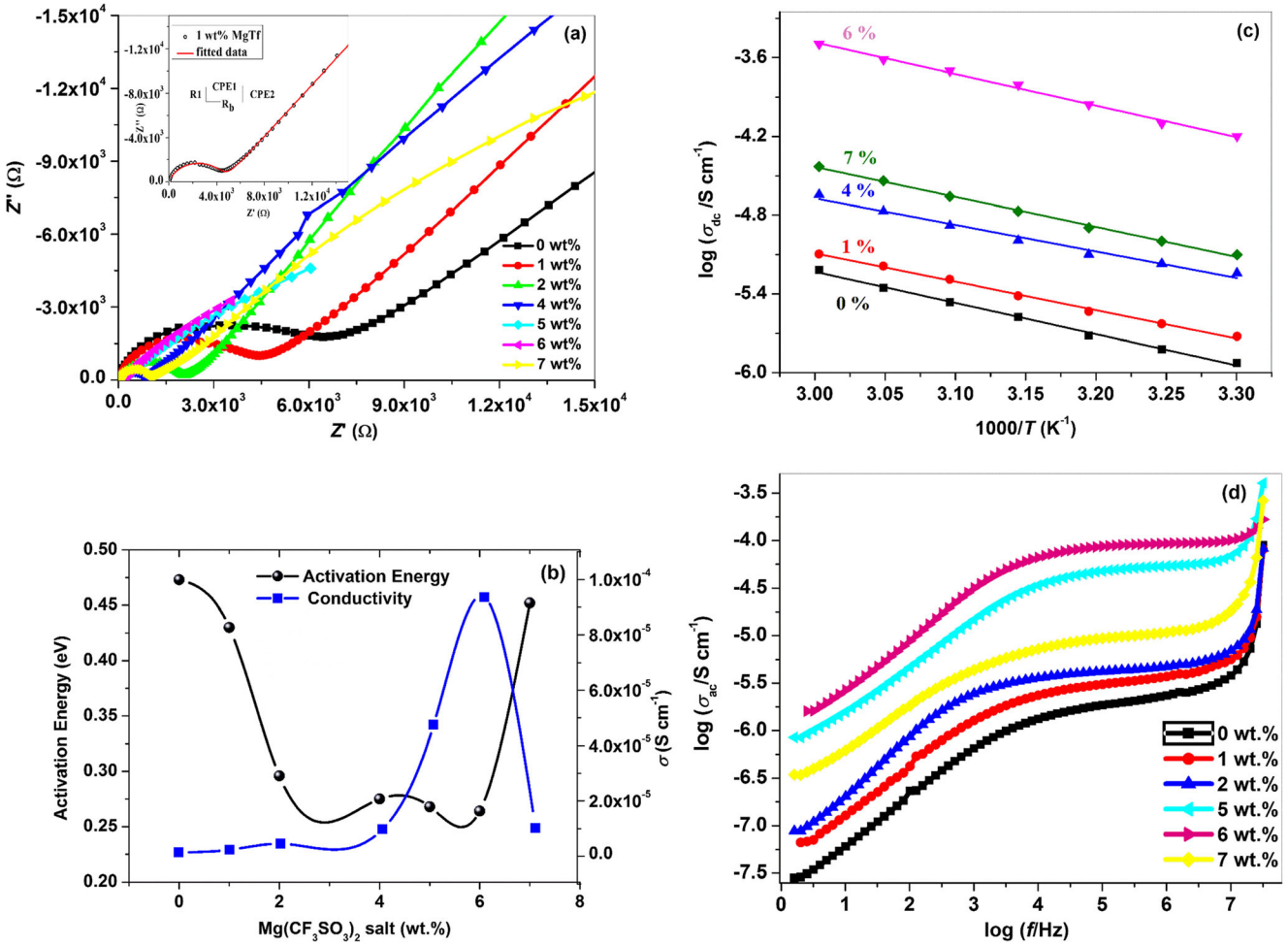

Fig. 5 **a** Nyquist plots of PEO + EMIM-BF_4 PEMs with different concentrations of $Mg(CF_3SO_3)_2$. **b** Variation of ionic conductivity as a function of $Mg(CF_3SO_3)_2$ salt concentration at room temperature. **c** Ionic conductivity as a function of temperature for PEMs containing $Mg(CF_3SO_3)_2$ salt concentration 0, 1, 4, 6, and 7 wt%. **d** Frequency dependent conductivity spectra of PEMs (PEO + EMIM-BF_4) + x wt% $Mg(CF_3SO_3)_2$ where $x = 0$, 1, 2, 5, 6, and 7

$$\sigma = \frac{t}{R_b A} \tag{2}$$

where σ is ionic conductivity of the electrolyte, t is thickness of the electrolyte specimen, R_b is bulk electrolyte resistance, and A is area of cross-section of the electrolyte specimen.

The lowest value of R_b is observed for 6 wt% salt concentration which corresponds to maximum ionic conductivity of 9.4×10^{-5} S cm^{-1} at 303 K. It is important to note that the lowest activation energy has been observed for this PEM with 6 wt% salt concentration. A decrease in ionic conductivity is observed for higher loading of 7 wt% $Mg(CF_3SO_3)_2$ salt concentration as shown in Fig. 5b . Such decreases in ionic conductivity and increase of activation energy values of PEM are attributed to ion-association/aggregation as reported previously [43]. As the salt concentration increases, the value of conductivity is increased monotonically up to 6 wt% at temperature 303 K. The decrease in activation energy and increase in the ionic conductivity with the increases of salt concentration may be related to the increase in the number of mobile charge carriers in the polymer electrolyte [44]. Figure 5c depicts the variation of ionic conductivity (σ) as a function of temperature for prepared PEMs. The straight line feature of σ versus $1000/T$ plots suggests that ion transport in the PEMs follows the typical Arrhenius behavior which can be ascribed by Arrhenius equation

$$\sigma = \sigma_0 \exp\left(\frac{-E_a}{kT}\right) \tag{3}$$

where σ_0 is pre-exponential factor, E_a is the activation energy, k is the Boltzmann constant, and T is absolute temperature [45]. The increase in conductivity with rise in temperature is possibly due to increased thermal movement of polymer chain segments and greater salt dissociation. However at lower temperature, dipole-dipole interaction increases the cohesive energy of polymer matrix thereby giving rising to lesser conductivity values. Such finding has been previously reported by Ramya et al. [46].

Figure 5 d shows the behavior of conductivity as a function of frequency for the six different compositions of the PEM system, (PEO + EMIM-BF_4) + x wt% $Mg(CF_3SO_3)_2$ where x = 0, 1, 2, 5, 6, and 7 wt%, at 303 K. It may be noted that the spectra depicts three distinct region viz., low frequency dispersion region corresponds to the electrode polarization, mid frequency plateau attributed to the dc conductivity, and the high frequency dispersion region which could infer the frequency dependent ion transport [47]. For each PEM, we observe conductivity dispersion in low frequency region arising from space charge polarization at the electrode-electrolyte interface. Mid frequency region indicates a frequency independent plateau corresponding to the dc conductivity of the PEMs. At the high frequency region, a sharp conductivity rise is noticed and such feature may be attributed to displacement of the ionic species under the effect of alternating field.

Dielectric studies

A study of the dielectric behavior of the PEM enables to understand the conductivity behavior of the electrolyte system. The ion conduction and relaxation mechanism of a PEM system can be investigated with the help of dielectric constant and dielectric loss. The complex permittivity ε^*or dielectric constant of a system is defined by:

$$\varepsilon^* = \varepsilon' - j\varepsilon'' = \varepsilon' - j\left(\frac{\sigma}{\omega\varepsilon_o}\right) \tag{4}$$

where ε' is real part of complex permittivity (also known as dielectric constant), ε'' is imaginary part of complex permittivity of material (also known as dielectric loss), σ is conductivity, ω is angular frequency, and $\varepsilon_o$is permittivity of free space. The mathematical expressions for ε' and ε'' are given by the following equations;

$$\varepsilon' = \frac{Z''}{\omega C_o\left(Z'^2 + Z''^2\right)} \tag{5}$$

$$\varepsilon'' = \frac{Z'}{\omega C_o\left(Z'^2 + Z''^2\right)} \tag{6}$$

where ω is angular frequency, C_o is capacitance in vacuum, and Z' and Z'' represent the real and imaginary parts of impedance for electrolyte system.

The value of tan δ has been determined using the following relation

$$\tan(\delta) = \frac{\varepsilon''}{\varepsilon'} = \frac{Z'}{Z''} \tag{7}$$

The variation of dielectric constant (ε') and tangent loss (tan δ) as a function of frequency is shown in Fig. 6a and b for different PEMs. Increase in dielectric constant (ε') at lower frequency region may be ascribed as space charge polarization due to accommodation or build-up of charges near the electrode-electrolyte interface [48–50]. This is because of ion or dipoles are able to orient themselves in the direction of applied reversal AC field at lower frequency region. Whereas, at the higher frequency region, there is occurrence of the fast periodic reversal of the applied field and therefore dipoles have no time to orient themselves. In view of this, ε' and tan (δ) decrease rapidly and approach close to zero at the high frequency portion. Another conclusion can be drawn from Fig. 6a that the value of ε' is increasing with increasing the amount of $Mg(CF_3SO_3)_2$ salt from 0 to 6 wt%, whereas reverse trend has been observed for system with higher $Mg(CF_3SO_3)_2$ concentration. The highest values of ε' for the (PEO + EMIM-BF_4) + 6 wt% $Mg(CF_3SO_3)_2$ PEM is noticed. This may be due to increase in the charge carrier density with increasing the salt concentrations [51].

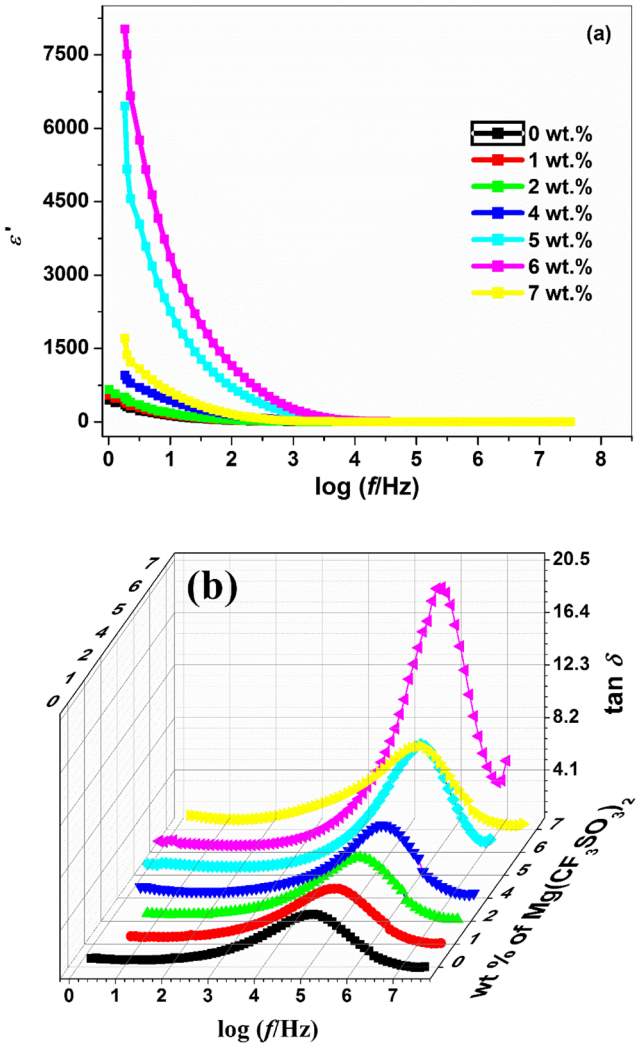

Fig. 6 Frequency-dependent **a** dielectric constant (ε') and **b** tan δ for (PEO + EMIM-BF_4) + x wt% $Mg(CF_3SO_3)_2$ where, x = 0, 1, 2, 4, 5, 6, and 7 at 303 K

Figure 6b shows tan (δ) versus log (f) for (PEO + EMIM-BF_4) + x wt% $Mg(CF_3SO_3)_2$ where x = 0, 1, 2, 4, 5, 6, and 7 at 303 K. The plot consists of a peak which shifts towards the higher frequency side with increasing the concentration of $Mg(CF_3SO_3)_2$ salt up to 6 wt%. Beyond this concentration, the maxima of peak shift towards lower frequency side. The shift in the peak indicates the relaxation phenomenon is occurring. The lowest relaxation time is observed for the optimized highest conducting PEM. This might be due to increase in the amorphous nature of the PEM with increasing amount of salt through which polymer chains can easily orient themselves.

Modulus studies

The frequency response of electric modulus representation is an established technique utilized extensively to identify the electrical relaxation and the electrode polarization effect. Mathematically, electric modulus is given by the relation

$$M^* = \left(\frac{1}{\varepsilon^*}\right) = j\omega C_o Z^* = M' + jM'' \quad (8)$$

where the angular frequency $\omega = 2\pi f$ and C_o is the vacuum capacitance of the electrochemical cell, and M' and M'' denote the real and imaginary parts of the modulus M^*, respectively. A true electrical relaxation for the PEMs with various salt concentrations is usually identified by plotting the real M' and imaginary M'' part of electric modulus as a function frequency as presented in Fig. 7a and b . An almost zero value of M' at low frequency indicates the negligible contribution of the electrode polarization. Long tail at lower frequencies stipulates the large capacitance is associated with it [52, 53]. Whereas a considerable raise in M' values as well as a shift in peak maximum towards the higher frequency region in observed as salt concentration increases up to 6 wt% $Mg(CF_3SO_3)_2$. A similar trend has been observed in the imaginary part (M'') of the electrical modulus. The shift in peak maximum with increasing the salt concentrations up to 6 wt%. This behavior indicates the occurrence of charge carriers hopping and relaxation phenomena due to decrease in the crystalline nature of PEM system with addition of more amount of salt concentration up to 6 wt%. Similar kind of behavior has also been reported by the Karmakar et al. [54].

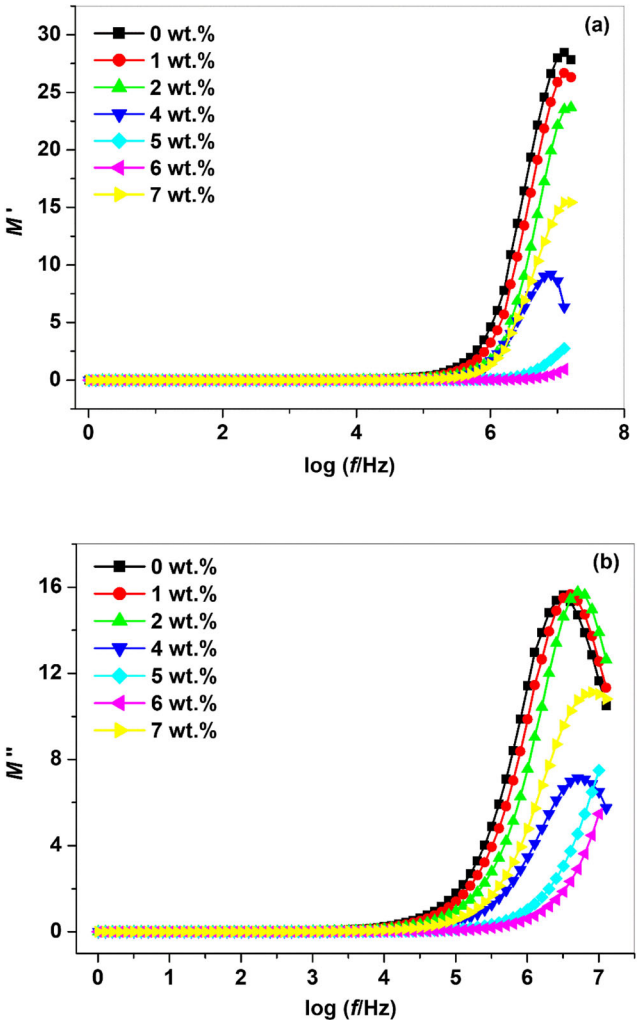

Fig. 7 Frequency-dependent **a** real part of modulus (M') and **b** imaginary part of modulus (M'') for (PEO + EMIM-BF_4) + x wt% $Mg(CF_3SO_3)_2$ where, x = 0, 1, 2, 4, 5, 6, and 7 at 303 K

Ion transport studies

Total ion transport number

The total ion transference number (t_{ion}) determines the contribution of ions in the total conductivity of PEM system. The t_{ion} value for optimized PEM, (PEO + EMIM-BF_4) + 6 wt% $Mg(CF_3SO_3)_2$, was estimated using dc polarization technique [55, 56]. As a part of the technique, a dc potential of 0.5 V was applied to the cell configuration SS|PEM|SS (SS, stainless steel) and current was monitored as a function of time. The t_{ion} values were obtained using formula:

$$t_{ion} = \frac{(I_t - I_e)}{I_t} \quad (9)$$

where I_t and I_e are total and saturated currents, respectively.

A typical current vs time plot for cell assemblies, SS|PEM|SS and Mg|PEM|Mg, with optimized PEM is shown in Fig. 8a . In these cell assemblies, SS acts as ion blocking electrode and allows only electronic reversibility at electrolyte/SS interface, while Mg shows reversibility for Mg^{2+} ion at electrolyte/electrode interface. In the polarization curve, initially the current (I_t) is observed as 28.50 μA cm^{-2}, which suddenly drop and saturate at 0.30 μA cm^{-2} (I_e). The t_{ion} value, calculated using Eq. 9 is obtained as ~ 0.99. This suggests that the conductivity of the prepared PEM system is dominantly due to ions and it is electronically insulating.

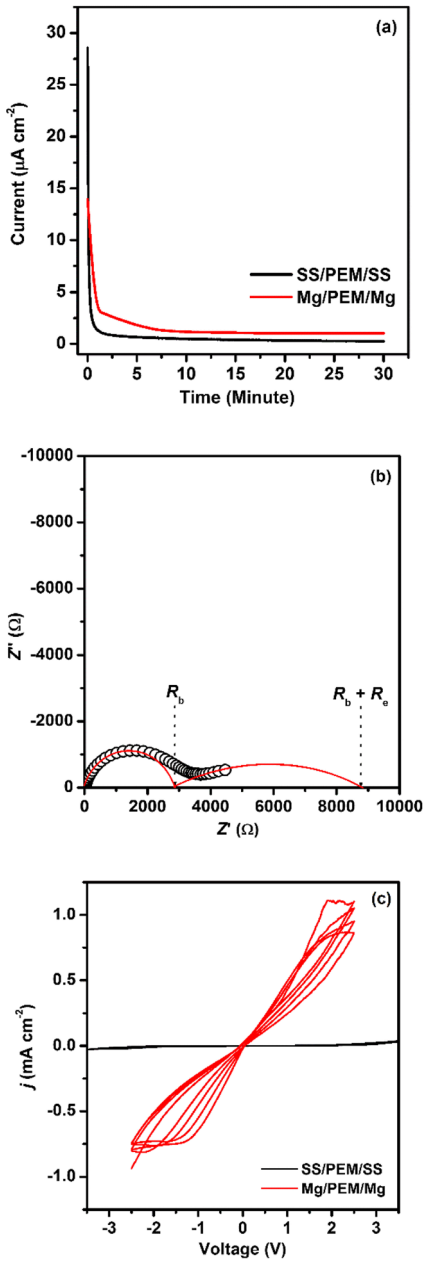

Fig. 8 **a** DC polarization curves for symmetrical cells; SS|PEM|SS and Mg|PEM|Mg. **b** Impedance curve for symmetrical cell; Mg|PEM|Mg. **c** Cyclic voltammograms of symmetrical cells, SS|PEM|SS and Mg|PEM|Mg using optimized PEM with composition (PEO + EMIM-BF_4) + 6 wt% $Mg(CF_3SO_3)_2$

Cation (Mg^{2+}) transport number

The magnesium transport number ($t_{Mg^{2+}}$) of the optimized PEM was estimated by a combination of ac impedance and dc polarization techniques as proposed by Watanabe et al. [57]. The impedance and polarization experiments were performed on the symmetrical Mg|PEM|Mg cell configuration and $t_{Mg^{2+}}$ values were calculated using formula:

$$t_{Mg^{2+}} = \frac{R_b}{\left(\frac{\Delta V}{I_s} - R_e\right)} \quad (10)$$

where R_b is the bulk resistance, R_e is the electrode/electrolyte interfacial resistance, I_s is the saturation current, and ΔV is the small constant voltage (20 mV) applied to the cell assembly.

In the polarization curve of Mg|PEM|Mg cell (Fig. 8a), the current receives saturation at relatively higher value (I_s = 1.03 μA cm^{-2}) as compared to SS|PEM|SS cell, which is an indicative of Mg^{2+} transport at electrolyte/Mg interface. In order to find $t_{Mg^{2+}}$ value for highest conducting composition, impedance plot of Mg|PEM|Mg cell is obtained (Fig. 8b). As illustrated in the figure, the bulk resistance (R_b) and electrode/electrolyte interfacial resistance (R_e) are obtained as 2864 and 5963 Ω, respectively. The $t_{Mg^{2+}}$ value, calculated using Eq. 10, is obtained as 0.22 for the highest conducting optimized composition.

In order to confirm Mg^{2+} conduction in the prepared PEM system and to assess its electrochemical stability, CV was performed on the two symmetrical cells, SS|PEM|SS and Mg|PEM|Mg at a scan rate of 5 mV s^{-1} (Fig. 8c). In the voltammogram of the cell with SS electrode, no anodic or cathodic peak is observed and also the current values are insignificant. This reflects a significantly high electrochemical stability window of the prepared PEM system. However, the voltammogram of Mg|PEM|Mg cell shows several times high current values with a couple of reversible redox peaks corresponding to cathodic deposition and anodic oxidation of Mg^{2+} at electrolyte/Mg interface. This shows the good reversibility of the Mg^{2+}/Mg redox couple in cell. In order to, further, confirm the electrochemical stability window, LSV was

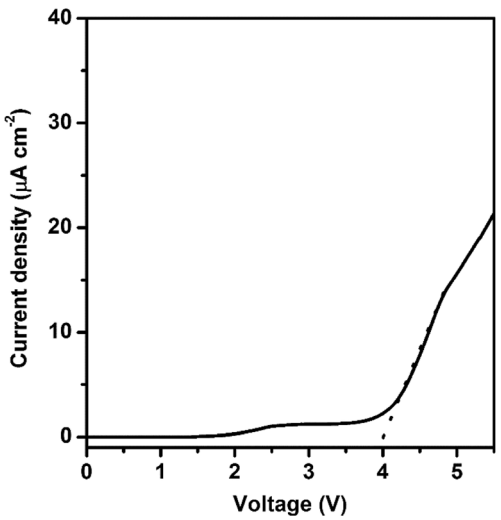

Fig. 9 Linear sweep voltammogram for PEM with composition (PEO + EMIM-BF_4) + 6 wt% $Mg(CF_3SO_3)_2$ in the cell configuration SS|PEM|Mg at a scan rate of 5 mV s^{-1}

performed on the highest conducting composition of the PEM system at a scan rate of 5 mV s^{-1} using SS as a working electrode and magnesium as a combined reference and counter electrode (Fig. 9). The LSV trace confirms the electrochemical stability window the highest conducting composition as ~4.0 V. These observations confirm the Mg^{2+} ion conductivity in the prepared PEM system with significant electrochemical stability. This assessment is an indicative of the potential applicability of the prepared PEMs in electrochemical devices especially the supercapacitors and batteries.

Conclusion

The prepared PEO + EMIM-BF_4 + $Mg(CF_3SO_3)_2$ films have been characterized using XRD, AFM, FTIR, and DSC studies. AFM analysis demonstrates minimum roughness height for optimized PEM with 6 wt% of $Mg(CF_3SO_3)_2$ concentration. FTIR analysis shows coordination of $EMIM^+/Mg^{2+}$ with ether oxygen of PEO and complexation among PEO/EMIM-BF_4/$Mg(CF_3SO_3)_2$. DSC study shows decrease in T_m on increasing $Mg(CF_3SO_3)_2$ concentration suggesting an increase of polymer chain flexibility. From the Nyquist plot, the highest ionic conductivity (~9.4×10^{-5} S cm^{-1}) is observed for optimized PEM with 6 wt% of $Mg(CF_3SO_3)_2$. The dc conductivity variation with temperature shows typical Arrhenius behavior for all PEMs. Dielectric studies depict increased values of dielectric constant (ε') at lower frequencies while the peak of dielectric loss (ε'') shifts towards higher frequency side with the addition of salt up to 6 wt% in the electrolyte films. Modulus studies indicate occurrence of charge carriers hopping and relaxation phenomenon in the PEMs films on adding $Mg(CF_3SO_3)_2$. The peak shift in M'' spectra suggested the decrease in relaxation time with the addition of salt up to 6 wt%. Total ion transport number is close to unity for all electrolytic films which indicates the conductivity is dominantly due to ions and it is electronically insulating. The Mg^{2+} conduction is confirmed using cyclic voltammetry study and Mg^{2+} transport number is determined to be 0.22 for the optimized (6 wt%) PEM. The observed changes in ionic conduction, relaxation parameters, and electrochemical performances with the variation of salt concentration suggest that PEO + EMIM-BF_4 + $Mg(CF_3SO_3)_2$ system may be a good electrolyte for battery applications.

Acknowledgments Deepak Kumar thanks and acknowledges "The M.S. University of Baroda," Vadodara, Gujarat, India. He also acknowledge encouragement and support received from Electronics and Mechanical Engineering School, Affiliated to Gujarat Technological University, Under Corps of EME, Ministry of Defence, Government of India.

Funding information Kuldeep Mishra acknowledges the funding (File No YSS/2015/001234) from Science and Engineering Research Board (SERB) New Delhi, India.

References

1. Deng D (2015) Li-ion batteries: basics, progress, and challenges. Energy Sci & Eng 3:385–418
2. Huang B, Pan Z, Su X, An L (2018) Recycling of lithium-ion batteries: recent advances and perspectives. J Power Sources 399: 274–286
3. Zubi G, López RD, Carvalho M, Pasaoglu G (2018) The lithium-ion battery: state of the art and future perspectives. Renew Sust Energ Rev 89:292–308
4. Vignarooban K, Kushagra R, Elango A, Badani P, Mellander BE, Xu X, Tucker TG, Nam C, Kannan AM (2016) Current trends and future challenges of electrolytes for sodium-ion batteries. Int J Hydrog Energy 41:2829–2846
5. Kumar D, Rajouria SK, Kuhar SB, Kanchan DK (2017) Progress and prospects of sodium-sulfur batteries: a review. Solid State Ionics 312:8–16
6. Deivanayagam R, Ingram BJ, Yassar RS (2019) Progress in development of electrolytes for magnesium batteries. Energy Storage Mater 21:136–153
7. Li H, Ma L, Han C, Wang Z, Liu Z, Tang Z, Zhi C (2019) Advanced rechargeable zinc-based batteries: recent progress and future perspectives. Nano Energy 62:550–587
8. Niu X, Li L, Qiu J, Yang J, Huang J, Wu Z, Zou J, Jiang C, Gao J, Wang L (2019) Salt-concentrated electrolytes for graphite anode in potassium ion battery. Solid State Ionics 341:115050
9. Zafar ZA, Imtiaz S, Li R, Zhang J, Razaq R, Xin Y, Li Q, Zhang Z, Huang Y (2018) A super-long life rechargeable aluminum battery. Solid State Ionics 320:70–75
10. Kong L, Yan C, Huang JQ, Zhao MQ, Titirici MM, Xiang R, Zhang Q (2018) A review of advanced energy materials for magnesium–sulfur batteries. Energy Environ Mater 1:100–112
11. Saha P, Datta MK, Velikokhatnyi OI, Manivannan A, Alman D, Kumta PN (2014) Rechargeable magnesium battery: current status and key challenges for the future. Prog Mater Sci 66:1–86
12. Angell CA (2017) Polymer electrolytes—some principles, cautions, and new practices. Electrochim Acta 250:368–375
13. Wang Y, Sokolov AP (2015) Design of superionic polymer electrolytes. Current Opin Chem Eng 7:113–119
14. Lu D, Liu H, Huang T, Xu Z, Ma L, Yang P, Qiang P, Zhang F, Wu D (2018) Magnesium ion based organic secondary batteries. J Mater Chem A 6:17297–17302
15. Mohanta J, Padhi DK, Si S (2018) Li-ion conductivity in PEO-graphene oxide nanocomposite polymer electrolytes: a study on effect of the counter anion. J Appl Polym Sci 135:46336
16. Ma Z, MacFarlane DR, Kar M (2019) Mg cathode materials and electrolytes for rechargeable Mg batteries: a review. Batteries Supercaps 2:115–127
17. Zardalidis G, Ioannou E, Pispas S, Floudas G (2013) Relating structure, viscoelasticity, and local mobility to conductivity in PEO/LiTf electrolytes. Macromolecules 46:2705–2714
18. Shobukawa H, Tokuda H, Susan MABH, Watanbe M (2005) Ion transport properties of lithium ionic liquids and their ion gels. Electrochim Acta 50:3872–3387
19. Ueki T, Watanabe M (2008) Macromolecules in ionic liquids: progress, challenges, and opportunities. Macromolecules 41:3739–3749
20. Tang J, Muchakayala R, Song S, Wang M, Kumar KN (2016) Effect of $EMIMBF_4$ ionic liquid addition on the structure and ionic conductivity of $LiBF_4$-complexed PVdF-HFP polymer electrolyte films. Polym Test 50:247–254
21. Aziz SB, Woo TJ, Kadir MFZ, Ahmed HM (2018) A conceptual review on polymer electrolytes and ion transport models. J Sci: Adv Mater Devices 3:1–17
22. Chaurasia SK, Singh RK, Chandra S (2011) Dielectric relaxation and conductivity studies on (PEO:LiClO4) polymer electrolyte with

added ionic liquid [BMIM][PF_6]: evidence of ion–ion interaction. J Polym Sci B Polym Phys 49:291–300
23. Chaurasia SK, Singh RK, Chandra S (2011) Ion–polymer and ion–ion interaction in PEO-based polymer electrolytes having complexing salt $LiClO_4$ and/or ionic liquid, [BMIM][PF_6]. J Raman Spectrosc 42:2168–2172
24. Ren C, Liu M, Zhang J, Zhang Q, Zhan X, Chen F (2018) Solid-state single-ion conducting comb-like siloxane copolymer electrolyte with improved conductivity and electrochemical window for lithium batteries. J Appl Polym Sci 135:45848
25. Liebenow C (1998) A novel type of magnesium ion conducting polymer electrolyte. Electrochim Acta 43:1253–1256
26. Pandey GP, Agarwal RC, Hashmi SA (2011) Magnesium ion-conducting gel polymer electrolytes dispersed with fumed silica for rechargeable magnesium battery application. J Solid State Electrochem 15:2253–2264
27. Morita M, Yoshimoto N, Yakushiji S, Ishikawa M (2001) Rechargeable magnesium batteries using a novel polymeric solid electrolyte. Electrochem Solid-State Lett 4:177–179
28. Kumar GG, Munichandraiah N (2000) A gel polymer electrolyte of magnesium triflate. Solid State Ionics 128:203–210
29. Reddy MJ, Chu PP (2002) Ion pair formation and its effect in PEO: Mg solid polymer electrolyte system. J Power Sources 109:340–346
30. Sarangika HNM, Dissanayake MAKL, Senadeera GKR, Rathnayake RRDV, Pitawala HMJC (2016) Polyethylene oxide and ionic liquid-based solid polymer electrolyte for rechargeable magnesium batteries. Ionics 23(10):2829–2835. https://doi.org/10.1007/s11581-016-1870-3
31. Saroj AL, Singh RK, Chandra S (2014) Thermal, vibrational, and dielectric studies on PVP/$LiBF_4$ + ionic liquid [EMIM][BF_4]-based polymer electrolyte films. J Phys Chem Solids 75:849–857
32. Sharma J, Hashmi SA (2019) Magnesium ion-conducting gel polymer electrolyte nanocomposites: effect of active and passive nanofillers. Polym Compos 40:1295–1306
33. Wilkes JS, Zaworotko MJ (1992) Air and water stable I-ethyl-3-methylimidazolium based ionic liquids. J Chem Soc Chem Commun 965-967
34. Cooper EI, O'Sullivan EJM (1992) Proceedings of 8th international symposium on ionic liquids (Eds. R. J. Gale, G. Blomgren, and H. Kojima). The Electrochemical Society, Pennington, NJ, p 386
35. Maurya KK, Srivastava N, Hashmi SA, Chandra S (1992) Proton conducting polymer electrolyte: II poly ethylene oxide + NH_4l system. J Mater Sci 27:6357–6364
36. Chaurasia SK, Saroj AL, Shalu SVK, Tripathi AK, Gupta AK, Verma YL, Singh RK (2015) Studies on structural, thermal and AC conductivity scaling of PEO-$LiPF_6$ polymer electrolyte with added ionic liquid [$BMIMPF_6$]. AIP Adv 5:077178
37. Maruthupandy M, Anand M, Maduraiveran G, Suresh S, Beevi ASH, Priya RJ (2016) Adv Nat Sci Nanosci Nanotechnol 7:045011 (9pp)
38. Parthiban V, Akula S, Peera SG, Islam N, Sahu AK (2016) Proton conducting Nafion-sulfonated graphene hybrid membranes for direct methanol fuel cells with reduced methanol crossover. Energy Fuel 30:725–734
39. Chaurasia SK, Singh RK, Chandra S (2011) Structural and transport studies on polymeric membranes of PEO containing ionic liquid, EMIM-TY: evidence of complexation. Solid State Ionics 183:32–39
40. Pasaribu MH, Arcana IM, Wahyuningrum D (2015) Molecular structure, vibrational spectra, and hydrogen bonding of the ionic liquid 1-ethyl-3-methyl-1H-imidazolium tetrafluoroborate. AIP Conf Proc 1677:070014
41. Skin JH, Kim KW, Ahn HJ, Ahn JH (2002) Electrochemical properties and interfacial stability of $(PEO)_{10}LiCF_3SO_3$–Ti_nO_{2n-1} composite polymer electrolytes for lithium/sulfur battery. J Mater Sci Eng B 95:148–156
42. Mishra K, Hashmi SA, Rai DK (2014) Protic ionic liquid-based gel polymer electrolyte: structural and ion transport studies and its application in proton battery. J Solid State Electrochem 18:2255–2266
43. Kumar D, Hashmi SA (2010) Ion transport and ion–filler-polymer interaction in poly(methyl methacrylate)-based, sodium ion conducting, gel polymer electrolytes dispersed with silica nanoparticles. J Power Sources 195:5101–5108
44. Ramesh S, Lu S (2011) Effect of lithium salt concentration on crystallinity of poly (vinylidene fluoride-co-hexafluoropropylene)-based solid polymer electrolytes. J Mol Struct 994:403–409
45. Pradhan DK, Choudhary RNP, Samantary BK (2008) Studies of dielectric relaxation and AC conductivity behavior of plasticized polymer nanocomposite electrolytes. Int J Electrochem Sci 3:597–608
46. Ramya CS, Pandian SS, Savitha T, Hirankumar G, Angelo PC (2007) Vibrational and impedance spectroscopic study on PVP–NH4SCN based polymer electrolytes. Phys B Condens Matter 393:11–17
47. Osman Z, Ghazali M, Othman L, Isa K (2012) AC ionic conductivity and DC polarization method of lithium ion transport in PMMA–LiBF4 gel polymer electrolytes. Result Phy 2:1–4
48. Kumar D, Kanchan DK (2019) Dielectric and electrochemical studies on carbonate free Na-ion conducting electrolytes for sodium-sulfur batteries. J Energy Storage 22:44–49
49. Gohel K, Kanchan DK (2018) Ionic conductivity and relaxation studies in PVDF-HFP:PMMA-based gel polymer blend electrolyte with LiClO4 salt. J Adv Dielect 8:1850005
50. Al-Gunaid MQA, Saeed AMN (2018) Effects of the electrolyte content on the electrical permittivity, thermal stability, and optical dispersion of poly(vinyl alcohol)–cesium copper oxide–lithium perchlorate nanocomposite solid-polymer electrolytes. J ApplPolym Sci 135:45852
51. Woo HJ, Majid SR, Arof AK (2012) Dielectric properties and morphology of polymer electrolyte based on poly (ε-caprolactone) and ammonium thiocyanate. Mater Chem Phys 134:755–761
52. Gohel K, Kanchan DK (2019) Effect of PC: DEC plasticizers on structural and electrical properties of PVDF–HFP: PMMA based gel polymer electrolyte system. J Mater Sci Mater Electron 30:12260–12268
53. Rathika R, Suthanthiraraj SA (2016) Ionic interactions and dielectric relaxation of PEO/PVDF-Mg[(CF3SO2)2N2] blend electrolytes for magnesium ion rechargeable batteries. Macromol Res 24:422–428
54. Karmakar A, Ghosh A (2012) Dielectric permittivity and electric modulus of polyethylene oxide (PEO)–LiClO4 composite electrolytes. Curr Appl Phys 12:539–543
55. Hashmi SA, Chandra S (1995) Experimental investigations on a sodium-ion-conducting polymer electrolyte based on poly (ethylene oxide) complexed with $NaPF_6$. J Mater Sci Eng B 34:18–26
56. Wagner JB Jr, Wagner C (1957) Electrical conductivity measurements on cuprous halides. J Chem Phys 26:1597
57. Watanabe M, Nagano S, Sanui K, Ogata N (1988) Estimation of Li^+ transport number in polymer electrolytes by the combination of complex impedance and potentiostatic polarization measurements. Solid State Ionics 28-30:911–917